



HHS Public Access

Author manuscript

J Am Chem Soc. Author manuscript; available in PMC 2022 February 03.

Published in final edited form as:

J Am Chem Soc. 2021 September 22; 143(37): 15358–15368. doi:10.1021/jacs.1c07018.

Coordination of the Copper Centers in Particulate Methane Monooxygenase: Comparison between Methanotrophs and Characterization of the Cu_C Site by EPR and ENDOR Spectroscopies

Richard J. Jodts,

Departments of Chemistry and Molecular Biosciences, Northwestern University, Evanston, Illinois 60208, United States

Matthew O. Ross,

Departments of Chemistry and Molecular Biosciences, Northwestern University, Evanston, Illinois 60208, United States; Present Address: M.O.R.: Department of Chemistry, University of Chicago, Chicago, Illinois 60637

Christopher W. Koo,

Departments of Chemistry and Molecular Biosciences, Northwestern University, Evanston, Illinois 60208, United States

Peter E. Doan,

Departments of Chemistry and Molecular Biosciences, Northwestern University, Evanston, Illinois 60208, United States

Amy C. Rosenzweig,

Departments of Chemistry and Molecular Biosciences, Northwestern University, Evanston, Illinois 60208, United States

Brian M. Hoffman

Departments of Chemistry and Molecular Biosciences, Northwestern University, Evanston, Illinois 60208, United States

Abstract

In nature, methane is oxidized to methanol by two enzymes, the iron-dependent soluble methane monooxygenase (sMMO) and the copper-dependent particulate MMO (pMMO). While sMMO's diiron metal active site is spectroscopically and structurally well-characterized, pMMO's copper sites are not. Recent EPR and ENDOR studies have established the presence of two monocopper sites, but the coordination environment of only one has been determined, that within the PmoB

Corresponding Authors Amy C. Rosenzweig – Departments of Chemistry and Molecular Biosciences, Northwestern University, Evanston, Illinois 60208, United States; amy@northwestern.edu; **Brian M. Hoffman** – Departments of Chemistry and Molecular Biosciences, Northwestern University, Evanston, Illinois 60208, United States; bmh@northwestern.edu.

Supporting Information

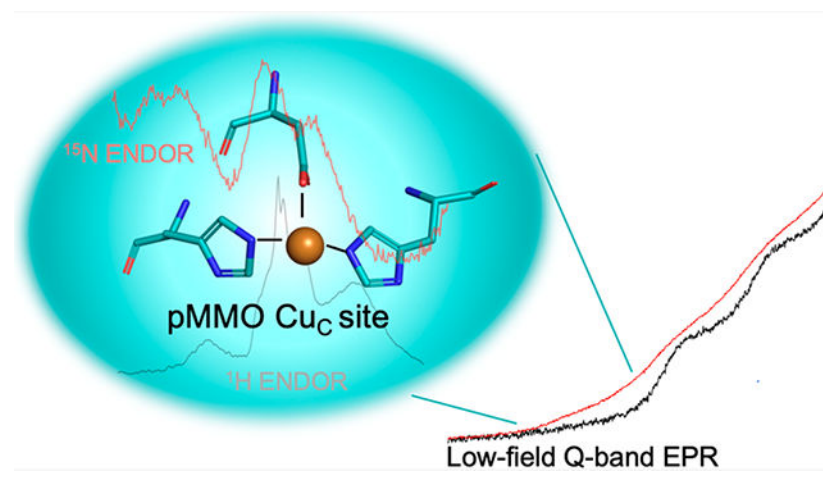
The Supporting Information is available free of charge at <https://pubs.acs.org/doi/10.1021/jacs.1c07018>.

Supporting methods {[Cu(NH₃)₄]²⁺ preparation and DFT} and figures (EPR and ENDOR spectra and PESTRE measurements) (PDF)

The authors declare no competing financial interest.

subunit and denoted Cu_B. Moreover, this recent work only focused on a type I methanotrophic pMMO, while previous observations of the type II enzyme were interpreted in terms of the presence of a dicopper site. First, this report shows that the type II *Methylocystis* species strain Rockwell pMMO, like the type I pMMOs, contains two monocopper sites and that its Cu_B site has a coordination environment identical to that of type I enzymes. As such, for the full range of pMMOs this report completes the refutation of prior and ongoing suggestions of multicopper sites. Second, and of primary importance, EPR/ENDOR measurements (a) for the first time establish the coordination environment of the spectroscopically observed site, provisionally denoted Cu_C, in both types of pMMO, thereby (b) establishing the assignment of this site observed by EPR to the crystallographically observed metal-binding site in the PmoC subunit. Finally, these results further indicate that Cu_C is the likely site of biological methane oxidation by pMMO, a conclusion that will serve as a foundation for proposals regarding the mechanism of this reaction.

Graphical Abstract



INTRODUCTION

Copper-dependent monooxygenase enzymes exploit the Cu(I)/Cu(II) redox couple to activate O₂ and insert one oxygen atom into organic substrates with strong C—H bonds, including the α carbon of glycine (C—H bond enthalpy, 87 kcal/mol),¹ polysaccharides (~100 kcal/mol),² and methane, with the strongest C—H bond (105 kcal/mol).³ The enzymes that oxidize these three substrates, respectively peptidylglycine α -hydroxylating monooxygenase (PHM),⁴ lytic polysaccharide monooxygenases (LPMOs), and particulate methane monooxygenase (pMMO), have been studied intensively with the goal of elucidating their chemical mechanisms. Members of the PHM family contain two well-characterized monocopper centers⁵ (denoted as Cu_M and Cu_H),⁴ while LPMO enzymes feature a single histidine brace-coordinated mononuclear copper active site.^{6,7} By contrast, mechanistic characterization of pMMO has been hindered by the absence of a molecular understanding of its active site location, nuclearity, and coordination environment.^{3,8} Such details are not only a prerequisite for mechanistic characterization but are also crucial if pMMO is to be utilized in biotechnological applications.⁹

pMMO is an integral-membrane enzyme comprising three subunits, PmoA, PmoB, and PmoC, arranged in a 300 kDa $\alpha_3\beta_3\gamma_3$ complex. On the basis of multiple pMMO crystal structures, two copper centers have emerged as potential active sites, one located in PmoB (Cu_B) and one located in PmoC (Cu_C) (Figure 1). The Cu_B site includes three histidine ligands, His29, His133, and His135, using type II *Methylocystis* (*Mc.*) species (sp.) strain (str.) Rockwell pMMO numbering, and in crystal structures has been modeled as being both mononuclear and dinuclear.¹⁰⁻¹³ However, several recent studies have firmly established its identity as mononuclear, including quantum refinement of the original *Methylococcus capsulatus* (Bath) pMMO crystal structure¹⁴ and native top-down mass spectrometry (nTDMS), which revealed the presence of a single copper ion localized to the amino terminus of PmoB.¹⁵ Most importantly, comprehensive electron paramagnetic resonance (EPR) and electron nuclear double resonance (ENDOR) spectroscopic analysis of *M. capsulatus* (Bath) whole cells cultivated on ¹⁵N isotopically enriched media indicated that the Cu_B site of this type I pMMO is mononuclear, revealed its coordination environment (three histidine ligands and an axially bound water), and showed that it is primarily present in the cell as $\text{Cu}_B(\text{II})$.¹⁶ The assignment of Cu_B as mononuclear is also supported by a recent reinvestigation of pMMO by X-ray absorption spectroscopy.¹⁷ Given the saturated equatorial coordination found for Cu_B and its presence as Cu(II) even in vivo, it is not likely to be the site of dioxygen and methane binding. In support of this conclusion, the three Cu_B histidine ligands are not conserved in a subset of pMMOs from type III methanotrophic verrucomicrobia.¹⁸

There is also a crystallographically identified metal-binding site in the PmoC subunit whose ligand set, which includes Asp129, His133, and His146 (Figure 1), is strictly conserved in pMMOs from all types of methanotrophs.¹⁸ In some pMMO structures, these three ligands coordinate a zinc ion from the crystallization buffer.^{10,11} In the absence of zinc, the site is occupied by copper.^{12,19} Furthermore, this site is adjacent to a highly conserved region of PmoC that is disordered in all the crystal structures,³ and nTDMS fragmentation of PmoC was not successful, underscoring the dearth of information about the properties of this site.¹⁵ EPR spectra of whole cells,¹⁶ anaerobically isolated membranes,²⁰ and isolated and purified type I *M. capsulatus* (Bath) pMMO in the presence of ascorbate reductant¹⁶ show only a signal from a single Cu(II) that is identified as the Cu_B site through ENDOR measurements. This indicates that if the metal-binding site in PmoC is indeed occupied by copper, it is present as Cu(I) in vivo and upon ascorbate reduction. Upon isolation and aerobic purification of *M. capsulatus* (Bath) pMMO, an EPR signal, provisionally denoted Cu_C , was detected and shown to be perturbed upon addition of nitrite, a pMMO inhibitor.¹⁶ However, although double electron electron resonance (DEER) measurements were consistent with the location of Cu_C in the PmoC subunit,¹⁶ the coordination environment of this copper ion was not determined and thus it was not definitively localized to the crystallographically observed copper site in PmoC.

Comprehensive EPR and ENDOR analysis of the Cu_B site was possible because it is conveniently monitored without overlap from the signal from Cu_C , which is readily reduced to Cu(I). However, the Cu_C EPR signal overlaps with that of Cu_B and cannot be observed unhindered by selective reduction of Cu_B . Moreover, our previous detailed EPR and ENDOR studies^{16,21} focused on pMMO from *M. capsulatus* (Bath), a type

I methanotroph, while the crystal structures guiding the interpretations include pMMOs from type II methanotrophs as well. These two methanotroph subclasses differ in cell morphologies, metabolic aspects, and lipid content,²² and their pMMOs exhibit structural differences, including an unidentified helix in the type II methanotroph pMMO structures.¹⁸ In addition, some type I methanotroph pMMOs contain a third “bis-His” copper site in the PmoB subunit¹⁰ that has not been observed in the type II methanotroph pMMOs.^{11,12,19}

In this report we show that the *Mc. sp. str. Rockwell* type II pMMO likewise contains two monocopper sites and that the electronic and coordination environment of the Cu_B site is conserved across pMMOs from both type I and type II methanotrophs. In doing so, we have collected EPR spectra of *Mc. sp. str. Rockwell* whole cells and of its purified/reduced type II pMMO and have used ¹H and ¹⁵N ENDOR to probe its Cu_B site, while carrying out additional measurements on the type I *M. capsulatus* (Bath) pMMO that reveal further details of the Cu_B site.

Of primary importance, ¹⁵N ENDOR studies of Cu_C were carried out on purified ¹⁵N, ⁶³Cu isotopically enriched pMMOs from both type I and type II methanotrophs by performing the measurements at fields where the Cu_C EPR signal does not overlap that of Cu_B. The results are the same for the two pMMO types and for the first time identify the presence of two histidyl ligands that coordinate the spectroscopically observed Cu_C, thereby showing that the spectroscopic Cu_C is appropriately assigned to the conserved and crystallographically observed metal-binding site in the PmoC subunit. ¹H ENDOR spectra in combination with the crystallographic data further suggest that Cu_C exhibits only three equatorial ligands and reveal that it is without axial ligation. The redox activity of the strictly conserved Cu_C site under conditions in which the Cu_B site remains oxidized, in conjunction with the nitrite interaction at the open coordination site of Cu_C,¹⁶ and the nTDMS data correlating the extent of copper binding to PmoC with activity¹⁵ together strongly suggest that Cu_C is the active site of biological methane oxidation by pMMO, a conclusion that lays the foundation for future mechanistic proposals and studies.

MATERIALS AND METHODS

Growth of *Mc. sp. str. Rockwell*.

To produce ⁶³CuSO₄ for enrichment growths, 50 mg aliquots of ⁶³CuO (Cambridge Isotope Laboratories) were dissolved in 1.5 mL of 3 M trace metal grade H₂SO₄ while heating at 60–80 °C and shaking at 300 rpm. The reaction was judged to be complete when no black ⁶³CuO particles were visible in the blue ⁶³CuSO₄ solution after several days. *Mc. sp. str. Rockwell* was grown in a 12 L fermentor as previously described²³ with minor adjustments. The medium consisted of 3.9 mM phosphate buffer, pH 6.8, 40 μM NaFe(III)EDTA, 1× trace element solution, 50 μM CuSO₄ (⁶³CuSO₄ prepared as described above was used for enrichment growths), and 1× nitrate mineral salts (NMS) (potassium ¹⁵N-nitrate, 99.98% enrichment, Cambridge Isotopes Laboratories, was used for isotope enriched samples) with a constant gas flow of ~1 L/min with a 1:4 methane:air gas mixture. The pH was maintained between 6.7 and 7.2 by addition of NaOH and H₂SO₄ as the growth proceeded. Cells were harvested by centrifugation (8000g for 35 min at 4 °C) at an OD₆₀₀ of 10.6 and were either

used immediately or frozen in liquid nitrogen and stored at $-80\text{ }^{\circ}\text{C}$. *M. capsulatus* (Bath) was grown and purified as described previously.¹³

Preparation of Whole Cell EPR and ENDOR Samples.

Freshly harvested cell paste (0.75 g) was resuspended in 50 mL of 12.2 mM dibasic sodium phosphate, 7.8 mM monobasic sodium phosphate, 5 mM magnesium chloride, pH 7.2. The resuspended cells were then centrifuged for 15 min at 10 000g. The supernatant was removed, and this wash procedure was repeated twice more. After the third spin, the cells were resuspended in 150 μL of the phosphate buffer and aliquoted into a Wilmad quartz X-band EPR tube (Sigma-Aldrich) and a custom quartz Q-band EPR tube. EPR samples were frozen in liquid nitrogen and stored in a liquid nitrogen Dewar until analysis.

Mc. sp. str. Rockwell pMMO Purification.

Frozen cells were resuspended in room-temperature 25 mM PIPES, 250 mM NaCl, pH 7.2 and lysed by sonication (1 s on, 1 s off, 10 min, 90% power setting). The cell debris was removed, and the membranes were isolated and washed as described previously.¹² The washed membranes were then resuspended in the PIPES buffer to 300 μM total protein, as determined by the Bio-Rad DC Lowry assay (with BSA as a standard), aliquoted in X-band and Q-band EPR tubes, and frozen in liquid nitrogen until analysis. Membranes were aliquoted, flash frozen in liquid nitrogen, and stored at $-80\text{ }^{\circ}\text{C}$ until further purification. *Mc. sp. str.* Rockwell pMMO was further purified and solubilized as described previously, but with PIPES instead of Tris buffer to avoid copper chelation by the buffer.¹² In brief, membranes were solubilized with *n*-dodecyl β -D-maltopyranoside (DDM), diluted with 25 mM PIPES, 0 M NaCl buffer, pH 7.2, and centrifuged at 100 000g for 1 h, and the soluble fraction was loaded onto a Source 15Q column (GE Healthcare). Fractions were assessed for purity by SDS PAGE, and those deemed pure were collected, concentrated, and flash frozen for later use. The protein concentration was determined by measuring the absorbance at 280 nm and using the extinction coefficient $7.66 \times 10^3\text{ M}^{-1}\text{ cm}^{-1}$.¹²

pMMO Nanodisc Reconstitution.

DDM-solubilized *M. capsulatus* (Bath) pMMO was incorporated into lipid nanodiscs with membrane scaffold protein (MSP1E3D1) and 1-palmitoyl-2-oleoylglycero-3-phosphocholine (POPC) using established methods.²⁴ pMSP1E3D1 (Addgene) was transformed into *Escherichia coli* BL21(DE3) cells and grown in TB media for 4 h at 37 $^{\circ}\text{C}$ until an OD_{600} of 2.1 was reached. Expression was induced by adding 1 mM IPTG, and cells were grown for another 4 h at 37 $^{\circ}\text{C}$ before pelleting and flash-freezing. Cells were resuspended in lysis buffer containing 40 mM Tris, pH 7.3, 250 mM NaCl, and 10 mM imidazole along with DNase, EDTA-free protease inhibitor cocktail (Roche), and 1% Triton X-100. Cells were lysed by sonication (10 min, 1 s on, 2 s off), and debris was removed by centrifugation at 10 000g for 30 min. The soluble fraction was applied to a Ni-NTA column and washed with 5 column volumes of lysis buffer containing 50 mM sodium cholate followed by 10 column volumes of lysis buffer. MSP1E3D1 was eluted with lysis buffer containing 250 mM imidazole. TEV protease was added at a ratio of 1:20, and the sample was dialyzed overnight at 4 $^{\circ}\text{C}$ against lysis buffer containing 1 mM EDTA. Cleaved MSP1E3D1 was collected from the Ni-NTA column flow-through and dialyzed overnight

against the PIPES buffer before concentrating and flash freezing. POPC solubilized in chloroform (Avanti) was dried to a thin layer in a glass vial against a stream of argon and then overnight in a vacuum desiccator. POPC was suspended at 50 mM in buffer containing 25 mM PIPES, pH 7.3, 250 mM NaCl, and 100 mM cholate by alternating heating at 60 °C, sonicating in an ultrasonic bath, and vortexing. Nanodisc components were mixed for 30 min at 4 °C at a ratio of 1:4:240 pMMO:MSP1E3D1:POPC. Biobeads SM-2 (Bio-Rad) washed with the PIPES buffer were added at 0.8 mg/mL and mixed end-over-end for 2 h before removal. Nanodiscs containing pMMO were purified using a Superose 6 10/300 column (Cytiva). EPR and ENDOR sample preparation is described below.

Preparation of Purified *Mc. sp. str. Rockwell* pMMO EPR and ENDOR Samples.

Samples of purified pMMO were loaded into X- and Q-band tubes and flash frozen. For partially reduced pMMO samples, an aliquot of pMMO was brought into a Coy anaerobic chamber and left for 24 h at 4 °C shaking at 400 rpm to remove dioxygen from the sample. Twelve equivalents of sodium ascorbic acid per 100 kDa protomer of pMMO was then added to the sample and allowed to incubate for 2 h at room temperature prior to freezing in an EPR tube anaerobically with liquid nitrogen and storing under liquid nitrogen. D₂O samples were produced by adding purified pMMO to D₂O buffer in a 1:10 000 dilution. This sample was kept for ~24 h at room temperature to exchange the protons within the enzyme and then concentrated with a 100 kDa MWCO Amicon concentrator. The concentration of purified *Mc. sp. str. Rockwell* pMMO was determined by using the absorbance at 280 nm and the calculated extinction coefficient of $7.66 \times 10^3 \text{ M}^{-1} \text{ cm}^{-1}$. The concentrated sample was then either frozen in an EPR tube or brought into the anaerobic chamber and reduced as described above.

EPR and ENDOR Measurements.

All CW (continuous wave) X-band EPR measurements were performed on a Bruker ESP-300 spectrometer with a liquid helium flow Oxford Instruments ESR-900 cryostat. EPR simulations were carried out in EasySpin.²⁵ Pulsed ENDOR measurements were collected at ~2 K on a spectrometer described previously, with SpinCore PulseBlaster ESR_PRO 400 MHz digital word generator and Agilent Technologies Acquiris DP235 500 MS/s digitizer using SpecMan4EPR software.^{26,27} For weakly coupled remote ¹⁵N ENDOR measurements, a Refocused Mims ENDOR (ReMims) pulse sequence [$\pi/2 - \tau_1 - \pi/2 - \text{TRF} - \pi/2 - \tau_2 - (\tau_1 + \tau_2) - \text{echo}$] was utilized in which TRF denotes the interval during which the RF was applied.²⁸ Strongly coupled ¹⁵N ENDOR measurements employed a Davies pulse sequence [$\pi - \text{TRF} - \pi/2 - \tau - \pi - \tau - \text{echo}$].²⁹ The 35 GHz CW ENDOR spectra were recorded on a modified Varian E-110 spectrometer equipped with a helium immersion dewar.³⁰ Cu_B site ¹H CW ENDOR spectra were collected using the field modulation detected stochastic ENDOR sequence³¹ in order to resolve the strongly coupled protons. The Cu_B ¹⁵N signals show peaks from two ligand types; to obtain the relative intensities of the two contributions, the signals were fit to a sum of Gaussians to determine their area ratio using the following equation:

$$f(x) = j \left\{ \frac{r}{\sigma' \sqrt{2\pi}} \exp \left[-\frac{(x - \mu')^2}{2\sigma'^2} \right] + \frac{(1-r)}{\sigma'' \sqrt{2\pi}} \exp \left[-\frac{(x - \mu'')^2}{2\sigma''^2} \right] \right\} \quad (1)$$

Here σ is a line width parameter and μ is the frequency of a peak, the primes distinguishing the two contributions; r is a fraction that defines the relative contributions of the two peaks; and j is a scaling factor to fit the experimental magnitudes.

Hyperfine Sign Determination.

To obtain the signs of the measured hyperfine couplings (more precisely to determine the sign of A/g_n), the *pulsed-ENDOR-saturation and recovery* (PESTRE) method was used at 35 GHz as described in detail previously.³²

RESULTS AND DISCUSSION

EPR Analysis of *Mc. sp. Str. Rockwell Whole Cells and Purified pMMO*.

CW X-band EPR spectra of ¹⁵N, ⁶³Cu enriched *Mc. sp. str. Rockwell* cells (Figure 2A) exhibit a strong signal from a single type 2 Cu(II) site ($g = [2.24, 2.07, 2.035]$, ⁶³Cu hyperfine splitting, $A_{||} = 580$ MHz) and a hyperfine pattern associated with the g_{\perp} region of the spectrum that arises from coordinated ¹⁵N. In addition, an isotropic $g \sim 2$ radical signal overlaps with the g_{\perp} region. This spectrum is consistent with previous EPR investigations of whole cell methanotrophs grown under copper-replete conditions^{33,34} and is identical to that assigned to the *M. capsulatus* (Bath) Cu_B site.¹⁶ When the membranes are isolated, the radical signal mostly disappears, the Cu_B signal persists, and a minority Cu(II) signal appears ($g = [2.31, 2.07, 2.05]$, ⁶³Cu $A_{||} = 440$ MHz coupling) (Figure 2B). The latter is shown by simulation to represent ~15% of the total Cu(II) signal and is assigned as the previously observed Cu_C signal.¹⁶ This spectrum is the first reported observation of the Cu_C signal in a membrane-bound type II pMMO. Once the enzyme is solubilized and purified, the Cu_C center becomes further oxidized, and simulations of the composite Cu_B and Cu_C spectrum show that within error this EPR signal comprises equal contributions from Cu_B and Cu_C (Figure 2C), the observed proportions varying somewhat with sample preparation.

An overlay of the spectra of solubilized/purified *M. capsulatus* (Bath) (type I) and *Mc. sp. str. Rockwell* (type II) pMMO [Figure S1, Supporting Information (SI)] shows that each site is identical between the two enzymes. This is the first report of preparations of a type II pMMO that, like the type I pMMO, exhibit both Cu_B and Cu_C signals in near equal occupancy and without additional adventitious Cu(II) signals (Figures S2 and S3, SI). Importantly, the presence of the Cu_C signal in the type II *Mc. sp. str. Rockwell* pMMO completely eliminates the possibility that this signal in the type I *M. capsulatus* (Bath) pMMO¹⁶ derives from the bis-His site in its PmoB subunit. The type II pMMOs, including *Mc. sp. str. Rockwell* pMMO, lack one of the two histidine residues that comprise this site.

Notably, there is an outlier crystal structure of *Mc. sp. str. Rockwell* pMMO in which the Cu_C site is occupied by Zn(II), which binds a fourth ligand, modeled as PmoC residue Glu201.¹⁰ In a recent computational study, this residue was assumed to be a ligand when

Cu(II) is bound in the Cu_C site.³⁵ However, this cannot be so. If such a four-coordinate “square planar” Cu(II) site with two nitrogen and two oxygen ligands were present, the ⁶³Cu A_{\parallel} value would differ significantly (closer to ~500 MHz)³⁶ from that observed for Cu_C (440 MHz). Correspondingly, the Cu_C site has a ratio $g_{\parallel}/A_{\parallel} = 156 \text{ cm} [A_{\parallel} = 1.46 \times 10^{-2} \text{ when expressed in wavenumbers (cm}^{-1}\text{)]$, whereas such square-planar complexes have ratios $g_{\parallel}/A_{\parallel} \sim 105\text{--}135 \text{ cm}$.³⁷ Thus, it is clear that Glu201 is only a ligand when Zn(II) occupies the site, and computational models based on its Cu coordination cannot³⁵ reflect the biological mechanism.

Addition of 8 equiv of ascorbate to purified *Mc. sp. str. Rockwell* pMMO eliminates the Cu_C signal, leaving the Cu_B signal with unchanged amplitude (Figure 2D) and indicating that the reduction potential of Cu_B is substantially more negative than that of Cu_C. An ability of the Cu_C site to cycle between the Cu(I) and Cu(II) states is consistent with proposals that it is the site of oxygen activation and methane conversion. Interestingly, we followed the previously published methods for isolation of *Mc. sp. str. Rockwell* pMMO and included as a necessary step the addition of CuSO₄ during cell lysis in order to achieve enzyme activity upon addition of detergent. An examination of purified samples by EPR (Figure S4, SI) that did not include this step shows only the Cu_B spectrum, similar to purified reduced enzyme (Figure 2D), without the Cu_C(II) signal seen when this step is included (Figure 2C). This observation provides further evidence that the presence of a copper ion in the Cu_C site is required for methane oxidation.

Investigation of the *Mc. sp. str. Rockwell* Cu_B Site by ENDOR Spectroscopy.

¹⁵N Pulsed ENDOR to Study Cu_B Nitrogen Coordination.—To further probe the molecular and electronic structure of the *Mc. sp. str. Rockwell* pMMO Cu_B site, we examined whole cell and purified/partially reduced samples by ENDOR. Our previous EPR and ENDOR studies of pMMO from the type I methanotroph *M. capsulatus* (Bath) clearly showed that the crystallographic Cu_B site is mononuclear.¹⁶ The use of quantitative ¹⁵N ENDOR to count nitrogen ligands to Cu_B established that it is coordinated by four nitrogenous ligands, three from histidyl imidazoles and one from the terminal NH₂ of His33 [*M. capsulatus* (Bath) pMMO numbering]. Using ¹⁵N, ⁶³Cu-enriched type II *Mc. sp. str. Rockwell* whole cells, Davies ENDOR at $g = 2.25$ reveals two ¹⁵N signals of $A \sim -48$ and -55 MHz (Figure 3, left). The PESTRE method shows that the ¹⁵N couplings (which correspond to the sign of A/gN) are negative, indicating a positive spin density on the coordinated ¹⁵N (Figure S5, SI). This is expected for in-plane Cu(II)-coordinated nitrogen. As reported previously for the type I *M. capsulatus* (Bath) pMMO, Gaussian fitting of the peaks using eq 1 yields areas with a 1:3 ratio, demonstrating that four nitrogens are coordinated to Cu_B, and that the signs of the couplings are equivalent as well.¹⁶

To identify the four Cu_B nitrogenous ligands, we probed for weakly coupled ¹⁵N signals from the remote (“backside”) nitrogens of histidyl imidazole ligands using the ReMims protocol.²⁸ Spectra collected at $g = 2.24$ show ¹⁵N signals exhibiting hyperfine couplings of ~ 1.7 and $\sim 2.4 \text{ MHz}$ (Figure 3, right) characteristic of such remote nitrogens. These signals have relative areas of 1:2, indicating that three of the four nitrogenous ligands to Cu_B in type II as in type I pMMOs are histidyl imidazoles, with the fourth then assignable to the

terminal amine. Finally, the values of the hyperfine couplings to both the coordinated and the remote ^{15}N of the histidines bound to the Cu_B sites are essentially the same for *M. capsulatus* (Bath) pMMO and *Mc. sp. str. Rockwell* pMMO, as is the coupling to the amine, demonstrating a complete equivalence of the Cu_B coordination in the two pMMO types. This identification of the coordination sphere of Cu_B in both types of pMMO, combined with other work identifying Cu_B as a monocopper site,^{14,15,17} is incompatible with a recent cryoelectron microscopy structure of *M. capsulatus* (Bath) pMMO.³⁸

Stochastic CW ^1H ENDOR of the Cu_B Site.—To refine our picture of the electronic and molecular structure of the Cu_B site, we employed 35 GHz field-modulated stochastic CW ^1H ENDOR on whole cell *Mc. sp. str. Rockwell*. The stochastic technique resolves line shapes better by eliminating the relaxation distortion of the CW ENDOR response, although with some sacrifice in signal intensity and with “inversion” of the distant-ENDOR responses with small couplings as a consequence of relaxation effects.

The single-crystal-like ^1H spectrum collected at the g_\parallel edge of the EPR spectrum for the Cu_B site (at a field corresponding to $g = 2.31$) shows a pair of broad responses that appear to be the superposition of two doublets with ^1H couplings of $A \sim 13$ and ~ 10 MHz (Figure 4, top). PESTRE measurements of the hyperfine coupling signs indicate that the intensity associated with the larger coupling exhibits a negative coupling, $A \sim -13$ MHz, while that for the smaller exhibits a positive one, $A \sim +10$ MHz (Figure S6, SI). These signals are lost upon exchange into a D_2O buffer (Figure 4, top, gray spectrum), indicating that they arise from two distinct classes of exchangeable protons. Similar observations were made for the type I *M. capsulatus* (Bath) enzyme,¹⁶ except that the previous study used only Davies pulsed ENDOR and did not resolve the presence of two distinct classes of exchangeable protons. In addition, there is a well-resolved doublet from nonexchangeable proton(s), with a coupling of $A \sim +5$ MHz (sign determined by PESTRE protocol), as well as (inverted) distant-ENDOR signals near ν_H .

The field-modulated detected stochastic ^1H ENDOR spectrum at g_\perp (Figure 4, bottom) again reveals two resolved large couplings from exchangeable protons, but in this case with the same (negative) sign, $A \sim -12$ and ~ -8 MHz (Figure S6, SI), as well as a nonexchangeable doublet with $A \sim +5$ MHz (Figure 4, bottom, gray spectrum). Again, the two large couplings resolved here in the stochastic experiment (most evident for the ν_+ peak) were observed in the previous study as a single broad peak with $A \sim 11$ MHz.¹⁴ The $\sim +5$ MHz coupling was assigned as a His C ϵ -H, consistent with the signs determined in this study.

The enhanced resolution of the exchangeable ^1H signals in the stochastic CW ^1H spectra allows for a reconsideration and further assignment of the large proton couplings. Previous ^{17}O ENDOR measurements showed the presence of an axial water on Cu_B ,¹⁴ and the present ^1H ENDOR measurements confirm this assignment. The appearance of a hyperfine-split doublet with $A \sim +10$ MHz at g_\parallel is characteristic of the protons of a water molecule bound axially to a square-planar Cu(II) site.^{37,39,40} At g_\perp , the exchangeable protons of this water molecule would give a coupling of $A \sim -5$ MHz; they are likely obscured by the signals from the nonexchangeable imidazole ring protons of the three histidine residues.

The exchangeable ^1H signals with $A \sim -13$ MHz at g_{\parallel} and $A \sim -12$ MHz at g_{\perp} are somewhat surprisingly assignable to the protons of the in-plane terminal amino group. Previous studies of protons of an amino group bound in-plane to Cu(II) reported couplings of these magnitudes, but without determination of signs.^{37,41,42} To better understand the hyperfine couplings to in-plane amine protons, we carried out a preliminary study of $[\text{Cu}(\text{II})(\text{NH}_3)_4]^{2+}$ using ^1H ENDOR. The preliminary results of field-modulated stochastic ENDOR and PESTRE show couplings of $A \sim -12$ MHz at g_{\parallel} and -12 MHz at g_{\perp} (Figure S7, SI), and DFT calculations of the ^1H hyperfine tensors gave corresponding results (see the SI). In retrospect, the previous lower-resolution ^1H ENDOR study of *M. capsulatus* (Bath) pMMO¹⁶ is consistent with the present, more complete study, leading to the conclusion that the Cu_B site is completely conserved across the type I and type II pMMOs.

Investigation of the *Mc. sp. Str. Rockwell* Cu_C Site by ENDOR Spectroscopy.

^{15}N Pulsed ENDOR of Cu_C Nitrogen Coordination.—Although purified pMMO exhibits strongly overlapping EPR signals from Cu_B and Cu_C , the enhanced “ g -spread” at Q-band versus X-band causes the difference in g_1 between the Cu_B and Cu_C sites to shift the four-line ^{63}Cu g_1 hyperfine pattern of Cu_C by ~ 250 G to lower field than that of Cu_B , as observed when overlaying the spectra of purified pMMO and in vivo pMMO (Figure 5). Within this low-field range, for the first time it is possible to exclusively probe the ^{15}N ENDOR of the Cu_C site without interference from signals that arise from Cu_B . The penalty paid for attempting such studies is the low Cu_C EPR signal intensity at these fields, which makes it necessary to use highly concentrated samples (>2 mM 100 kDa protomer) to obtain signals of reasonable signal/noise. Using such samples enabled us to obtain ^{15}N ENDOR spectra for the Cu_C site within the field range indicated in Figure 5 (inset, gray bracket region). A bonus of measurements taken within this field range is that these spectra are “single-crystal-like”,⁴³ meaning that they are selectively associated with the small subset of Cu_C sites oriented in the frozen sample so that the external field lies along the normal to the Cu_C ligand plane, a situation that yields the highest resolution and most easily analyzed signals.

Using an isotopically enriched, purified *Mc. sp. str. Rockwell* type II pMMO sample, ^{15}N Davies pulsed ENDOR was used to analyze the coordination environment and electronic structure of the Cu_C site. When the magnetic field is set within the “clean” low-field window (Figure 5), at a value corresponding to $g = 2.32$, the ^{15}N ENDOR spectrum of Cu_C exhibits resolved features that correspond to ^{15}N hyperfine couplings from two coordinating nitrogenous ligands, with couplings of $A \sim -46$ and -50 MHz (Figure 6, black); the negative signs were determined by the PESTRE technique as discussed for Cu_B above (Figure S8, SI). Spectra from an ^{15}N enriched, concentrated, purified type I pMMO sample from *M. capsulatus* (Bath) at this field reveal identical ^{15}N couplings (Figure S9, SI), signifying that the Cu_C nitrogen coordination is conserved between pMMOs from type I and II methanotrophs, as shown above for the Cu_B nitrogen coordination. The presence of two Cu_C ^{15}N ligands is also detected as hyperfine couplings in the X-band EPR spectrum (Figure S10, SI), analogous to the confirmation of four such ligands in the Cu_B site.¹⁴

As a control to ensure we were not observing signals from the Cu_B site, ENDOR spectra were collected at the same g -value from an ¹⁵N, ⁶³Cu *Mc. sp. str. Rockwell* whole-cell sample, which exhibits only a Cu_B EPR signal. There is no ¹⁵N ENDOR signal at this field (Figure 6, red spectrum), whereas the Cu_B signals are strong at higher fields, within the Cu_B envelope, thus confirming that the observed signals (Figure 6, red spectrum) derive exclusively from the Cu_C site.

Interestingly, the resolution of the ENDOR signal of both of the two Cu_C ¹⁵N ligands changes at still lower field (corresponding to $g = 2.34$; Figure S11, SI). This variation is attributable to differences in the orientations of their hyperfine tensors relative to the g -tensor, an indication of the low symmetry of the Cu_C coordination sphere (Figure S12, SI). The X-band EPR spectrum of the Cu_C site gives a ratio $g_{\parallel}/A_{\parallel} = 156$ cm (see above), which would suggest a distorted tetrahedral geometry.³⁷

To identify the two nitrogenous ligands to Cu_C revealed by the Q-band Davies pulsed ¹⁵N-ENDOR, we performed a ReMims ENDOR experiment to determine the presence and number of signals from the remote ¹⁵N of histidyl ligands, as done for the Cu_B site (Figure 3, right). The Cu_C ReMims ¹⁵N ENDOR spectra reveal one doublet associated with weakly coupled ¹⁵N, $|A| \sim 2$ MHz (Figure 7), typical for a remote nitrogen of a histidine residue. However, these peaks are broad compared to the remote ¹⁵N peaks for Cu_B, which is evident upon overlay with the peaks in Figure 3 (see Figure S13, SI). As shown in Figure 7, the spectrum is best interpreted as arising from unresolved doublets from two slightly inequivalent remote histidyl ¹⁵N ($|A| = 1.8, 2.1$ MHz), as expected for Cu_C bound to the two conserved histidine residues in the PmoC crystallographic site (Figure 1).

¹H ENDOR Analysis of the Cu_C Site.—We further investigated the Cu_C site by ¹H CW ENDOR. Spectra of concentrated, purified *Mc. sp. str. Rockwell* pMMO in H₂O and D₂O were again collected in the low-field window, at 10 600 G ($g = 2.34$) (Figure 8, upper). The results for this type II pMMO Cu_C site are indistinguishable from those obtained for the type I pMMO from *M. capsulatus* (Bath).¹⁶ The H₂O spectrum shows broad peaks from several doublets: a clearly resolved doublet with $A \sim +5$ MHz, where the sign has been determined by the PESTRE protocol (Figure S14, SI), and a pair of doublets with $A \sim 2$ and $|A| \sim 1$ MHz (Figure 8, upper, solid black). The sign of the first of these two was again determined by PESTRE; sign determination was not possible for the second.

Examination of a sample exchanged into D₂O buffer and incubated for 24 h at room temperature reveals loss of the doublet with $A \sim +5$ MHz, leaving a broad, ill-resolved feature extending to nearly $|A| \sim 5$ MHz. Although some of this signal may arise from residual H₂O after exchange, PESTRE shows a negative sign for $A \sim -2$ to -5 MHz (Figure 8, upper, dashed gray and Figure S14, SI), definitively showing that the signal arises from nonexchangeable protons. The exchangeable ~ 1 MHz doublet may well be associated with the remote N–H of the histidine residues⁴⁴ (Figure 7). The nonexchangeable doublets most likely arise from C ϵ or C δ protons of the histidine residues.⁴⁵

In the 2.6 Å resolution crystal structure of *Mc. sp. str. Rockwell* pMMO (PDB 4PHZ),¹² the electron density 3.3 Å from Cu_C is modeled as a solvent molecule axial to the Cu 2N1O

plane, but it is not coordinated to the copper ion. The exchangeable proton signal with $A \sim +5$ MHz likely is associated with this solvent molecule, aligning the X-ray and ENDOR measurements of Cu_C . This assignment revises the suggestion based on the interpretation of an ^{17}O ENDOR measurement on purified *M. capsulatus* (Bath) pMMO in buffer prepared with H_2^{17}O .¹⁶ The assignment is supported by additional examination of the ^{17}O ENDOR response (Figure S15, SI) and by the absence of signals attributable to coordinated ^{17}O at fields where the Cu_C EPR signal is not overlapped with that from Cu_B (Figure S16, SI).

The absence of any ^1H signals with $|A| > 5$ MHz at g_{\parallel} (Figure S17, SI) is additional evidence against a coordinated water for Cu_C ; if such a ligand were present, it would exhibit a ^1H doublet with $|A| \sim 10$ MHz,^{39,40} contrary to experiment. We therefore conclude that Cu_C does not have a coordinated water. The Cu_C signal might be imagined to derive from protons on a nearby arginine residue (Arg138, ~ 5 Å from Cu_C), but these are too remote to give rise to the observed coupling. We therefore attribute the exchangeable signal to the crystallographically observed ordered water within the secondary coordination sphere of Cu_C . The equivalence of the ^1H ENDOR measurements for the type I and type II pMMOs indicates that the solvent molecule near Cu_C is present in both, expanding the extent to which the site is highly conserved.

EPR and ENDOR Analysis of pMMO in Nanodiscs.—Because the Cu_C site adopts the Cu(I) state in vivo and cannot be examined by EPR, we sought to recreate a membrane environment in lipid nanodiscs, as recently used for nTDMS characterization of pMMO.¹⁵ The reconstitution of pMMO in nanodiscs in the presence of additional copper has led to higher enzymatic activity and higher copper loading of the PmoC subunit compared to detergent-solubilized pMMO.

The X-band EPR spectrum of purified *M. capsulatus* (Bath) pMMO reconstituted into nanodiscs is nearly identical to those of the purified enzyme¹⁶ in detergent [Figure S18 (SI) and Figure 2C]. However, as a result of the higher Cu_C copper loading in the nanodisc, the Cu_C EPR signal has a greater intensity than that of the detergent-purified sample. Thus, the $\text{Cu}_C(\text{II})$ coordination does not change despite the fact that it is within the transmembrane region adjacent to a part of PmoC that is disordered in the crystal structures and might be expected to have a different conformation in the nanodisc.

However, the overall environment of the Cu_C site is altered by nanodisc incorporation. The Cu_C ^1H ENDOR spectrum collected at the low magnetic field edge of the EPR spectrum of the nanodisc sample is dramatically different from that of pMMO in detergent (Figure 8, lower). The broad $A \sim +5$ MHz doublet seen for detergent-solubilized pMMO and assigned to protons from the noncoordinated distal water molecule is lost upon incorporation into the nanodisc. The remaining intensity in this frequency range corresponds to the signals in the D_2O sample of purified enzyme, which are nonexchangeable assigned to the histidine ligands (Figure 8, upper, gray). Thus, although the ligation to Cu_C is unchanged in the nanodisc, the solvent molecule near this site is lost.

We correspondingly tested for possible effects of nanodisc incorporation on the Cu_B site in the solvent-exposed PmoB subunit, using enzyme in which Cu_C has been reduced to the

Cu(I) state through the addition of 10 equiv of ascorbic acid per pMMO protomer. Both the X-band EPR spectrum (Figure S19, SI) and the ^1H ENDOR spectra (Figure S20, SI) are unchanged, indicating that the Cu_B ligation, including the presence of an axial water, is unchanged. Thus, the Cu_B site is essentially identical in vivo, in detergent-solubilized pMMO, and in pMMO reconstituted into nanodiscs, whereas the Cu_C surroundings are altered in the membrane-like environment of a nanodisc. Therefore, changes in pMMO activity in the different environments may be associated with changes in the Cu_C site.

CONCLUSION

Our EPR and ENDOR analysis of the type II *Mc. sp. str. Rockwell* pMMO provides several key insights into the pMMO copper centers. First, the Cu_B sites in pMMOs from type I and type II methanotrophs have identical molecular and electronic structures: each is a mononuclear site with four nitrogen ligands, comprising three histidyl imidazoles and one terminal amine. Given that Cu_B in vivo is coordinated to all the crystallographically identified ligands that are available in that site, this result definitively confirms the conclusion that this site contains a single Cu(II) ion.

In addition, an axial water associated with Cu_B is identified for the first time by its proton signals in stochastic CW ^1H ENDOR in parallel with PESTRE measurements. These results, combined with previous ^{17}O ENDOR on *M. capsulatus* (Bath) pMMO,¹⁶ are consistent with a square pyramidal geometry (Figure 9). The role of the Cu_B site and the potential functional significance of this axial water molecule, which is consistent with crystallographic^{12,14} and XAS¹⁷ data, remain unclear. The role of the histidine brace, a feature shared with LPMO, is also unclear. As a coordinatively saturated site that exists as Cu(II) in vivo, Cu_B is unlikely to be the site of methane oxidation. However, it is important for activity,⁴⁶ and possible roles in electron transfer or structural stabilization merit investigation.

Second and most important, we have obtained the first time definitive molecular and electronic structural information on the Cu_C site, previously uncharacterized by EPR because its signal overlaps with that of the Cu_B site. The ^{15}N ENDOR data reveal the presence of two histidine ligands. Supported by a prior DEER experiment on *M. capsulatus* (Bath) pMMO, this finding indicates that the copper ion corresponding to the spectroscopic EPR signal denoted Cu_C exhibits properties that are completely consistent with coordination by the three protein-derived ligands of the crystallographically observed Cu_C site: the two histidyl imidazoles of His133 and His146, along with the carboxylate of Asp129 (Figures 1, 9).

The ^1H ENDOR data expand this assignment by showing that the enzyme in detergent exhibits signals from a crystallographically observed nearby axial water molecule at a distance of $\sim 3 \text{ \AA}$ and that this water is lost when the enzyme is incorporated in the membrane-like environment of a nanodisc. The resulting presence of open Cu_C coordination sites provides space for dioxygen and methane to bind. Notably, LPMOs also have open coordination sites (occupied in crystal structures by chloride ions or water molecules) in the equatorial and axial positions,⁷ and substrate binding displaces an axial water molecule.⁴⁷ With this coordination environment, the pMMO Cu_C (I) complex would be expected to react

rapidly with dioxygen,⁴⁸ in keeping with the suggested role of Cu_C as the site of methane oxidation.

The loss of the noncoordinated, yet ordered, axial water molecule upon nanodisc incorporation is intriguing and perhaps not surprising given the location of Cu_C within the lipid bilayer. This water molecule may occupy a channel or pocket for methane and/or dioxygen diffusion and binding. Finally, it is worth noting that there are two conserved histidine residues in a crystallographically disordered region of PmoC not visible in any crystal structure. This unobserved sequence neighbors the crystallographic Cu_C site³ and could play a yet to be identified role in metal binding and enzyme function. Regardless, the detailed insight into the primary and secondary coordination sphere of the Cu_C site, which the present results suggest is the likely site of catalysis, provides a new foundation for probing the pMMO mechanism via computational and spectroscopic studies.

Supplementary Material

Refer to Web version on PubMed Central for supplementary material.

ACKNOWLEDGMENTS

We thank Prof. George Schatz (Northwestern) for use of his computational cluster for DFT calculations.

Funding

This work was supported by NIH grants GM118035 (A.C.R.) and GM11097 (B.M.H.) and by the NSF (MCB1908587 to B.M.H). R.J.J., M.O.R., and C.W.K were partially supported by NIH grant T32GM008382.

REFERENCES

- (1). Hioe J; Mosch M; Smith DM; Zipse H Dissociation energies of C α -H bonds in amino acids - a re-examination. *RSC Adv.* 2013, 3, 12403–12408.
- (2). Ipsen JO; Hallas-Møller M; Brander S; Lo Leggio L; Johansen KS Lytic polysaccharide monoxygenases and other histidine-brace copper proteins: structure, oxygen activation and biotechnological applications. *Biochem. Soc. Trans* 2021, 49, 531–540. [PubMed: 33449071]
- (3). Koo CW; Rosenzweig AC Biochemistry of aerobic biological methane oxidation. *Chem. Soc. Rev* 2021, 50, 3424–3436. [PubMed: 33491685]
- (4). Klinman JP The copper-enzyme family of dopamine β -monoxygenase and peptidylglycine α -hydroxylating monoxygenase: resolving the chemical pathway for substrate hydroxylation. *J. Biol. Chem* 2006, 281, 3013–3016. [PubMed: 16301310]
- (5). Eipper BA; Quon AS; Mains RE; Boswell JS; Blackburn NJ The catalytic core of peptidylglycine alpha-hydroxylating monoxygenase: investigation by site-directed mutagenesis, Cu X-ray absorption spectroscopy, and electron paramagnetic resonance. *Biochemistry* 1995, 34, 2857–2865. [PubMed: 7893699]
- (6). Quist DA; Diaz DE; Liu JJ; Karlin KD Activation of dioxygen by copper metalloproteins and insights from model complexes. *J. Biol. Inorg. Chem* 2017, 22, 253–288. [PubMed: 27921179]
- (7). Vu VV; Ngo ST Copper active site in polysaccharide monoxygenases. *Coord. Chem. Rev* 2018, 368, 134–157.
- (8). Ross MO; Rosenzweig AC A tale of two methane monoxygenases. *J. Biol. Inorg. Chem* 2017, 22, 307–319. [PubMed: 27878395]
- (9). Lawton TJ; Rosenzweig AC Methane-oxidizing enzymes: An upstream problem in biological gas-to-liquids conversion. *J. Am. Chem. Soc* 2016, 138, 9327–9340. [PubMed: 27366961]

- (10). Lieberman RL; Rosenzweig AC Crystal structure of a membrane-bound metalloenzyme that catalyses the biological oxidation of methane. *Nature* 2005, 434, 177–182. [PubMed: 15674245]
- (11). Smith SM; Rawat S; Telser J; Hoffman BM; Stemmler TL; Rosenzweig AC Crystal structure and characterization of particulate methane monooxygenase from *Methylocystis* species strain M. *Biochemistry* 2011, 50, 10231–10240. [PubMed: 22013879]
- (12). Sirajuddin S; Barupala D; Helling S; Marcus K; Stemmier TL; Rosenzweig AC Effects of zinc on particulate methane monooxygenase activity and structure. *J. Biol. Chem* 2014, 289, 21782–21794. [PubMed: 24942740]
- (13). Ro SY; Ross MO; Deng YW; Batelu S; Lawton TJ; Hurley JD; Stemmler TL; Hoffman BM; Rosenzweig AC From micelles to bicelles: Effect of the membrane on particulate methane monooxygenase activity. *J. Biol. Chem* 2018, 293, 10457–10465. [PubMed: 29739854]
- (14). Cao LL; Caldararu O; Rosenzweig AC; Ryde U Quantum refinement does not support dinuclear copper sites in crystal structures of particulate methane monooxygenase. *Angew. Chem., Int. Ed* 2018, 57, 162–166.
- (15). Ro SY; Schachner LF; Koo CW; Purohit R; Remis JP; Kenney GE; Liauw BW; Thomas PM; Patrie SM; Kelleher NL; Rosenzweig AC Native top-down mass spectrometry provides insights into the copper centers of membrane-bound methane monooxygenase. *Nat. Commun* 2019, 10, 2675. [PubMed: 31209220]
- (16). Ross MO; MacMillan F; Wang J; Nisthal A; Lawton TJ; Olafson BD; Mayo SL; Rosenzweig AC; Hoffman BM Particulate methane monooxygenase contains only mononuclear copper centers. *Science* 2019, 364, 566–570. [PubMed: 31073062]
- (17). Cutsail GE III; Ross MO; Rosenzweig AC; DeBeer S Towards a unified understanding of the copper sites in particulate methane monooxygenase: an X-ray absorption spectroscopic investigation. *Chem. Sci* 2021, 12, 6194–6209. [PubMed: 33996018]
- (18). Koo CW; Rosenzweig AC Particulate methane monooxygenase and the PmoD protein. In *Encyclopedia of Inorganic and Bioinorganic Chemistry*; John Wiley & Sons, Ltd., 2020; DOI: 10.1002/9781119951438.eibc2740.
- (19). Hakemian AS; Kondapalli KC; Telser J; Hoffman BM; Stemmler TL; Rosenzweig AC The metal centers of particulate methane monooxygenase from *Methylosinus trichosporium* OB3b. *Biochemistry* 2008, 47, 6793–6801. [PubMed: 18540635]
- (20). Choi DW; Antholine WE; Do YS; Semrau JD; Kisting CJ; Kunz RC; Campbell D; Rao V; Hartsel SC; DiSpirito AA Effect of methanobactin on the activity and electron paramagnetic resonance spectra of the membrane-associated methane monooxygenase in *Methylococcus capsulatus* Bath. *Microbiology* 2005, 151, 3417–3426. [PubMed: 16207923]
- (21). Culpepper MA; Cutsail GE 3rd; Gunderson WA; Hoffman BM; Rosenzweig AC Identification of the valence and coordination environment of the particulate methane monooxygenase copper centers by advanced EPR characterization. *J. Am. Chem. Soc* 2014, 136, 11767–11775. [PubMed: 25059917]
- (22). Semrau JD; Dispirito AA; Yoon S Methanotrophs and copper. *FEMS Microbiol. Lett* 2010, 34, 496–531.
- (23). Sirajuddin S; Rosenzweig AC Protocols for structural and functional analysis of particulate methane monooxygenase from *Methylocystis* species strain Rockwell (ATCC 49242). In *Hydrocarbon and Lipid Microbiology Protocols*; McGenity TJ, et al., Eds.; Springer-Verlag: Berlin, Heidelberg, 2016; pp 149–160.
- (24). Denisov IG; Grinkova YV; Lazarides AA; Sligar SG Directed self-assembly of monodisperse phospholipid bilayer nanodiscs with controlled size. *J. Am. Chem. Soc* 2004, 126, 3477–3487. [PubMed: 15025475]
- (25). Stoll S; Schweiger A EasySpin, a comprehensive software package for spectral simulation and analysis in EPR. *J. Magn. Reson* 2006, 178, 42–55. [PubMed: 16188474]
- (26). Davoust CE; Doan PE; Hoffman BM Q-band pulsed electron spin-echo spectrometer and its application to ENDOR and ESEEM. *J. Magn. Reson. Ser. A* 1996, 119, 38–44.
- (27). Epel B; Gromov I; Stoll S; Schweiger A; Goldfarb D Spectrometer manager: A versatile control software for pulse EPR spectrometers. *Concepts Magn. Reson., Part B* 2005, 26B, 36–45.

- (28). Doan PE; Hoffman BM Making hyperfine selection in Mims ENDOR independent of deadtime. *Chem. Phys. Lett* 1997, 269, 208–214.
- (29). Schweiger A; Jeschke G Principles of Pulse Electron Paramagnetic Resonance; Oxford University Press: Oxford, UK, 2001.
- (30). Werst MM; Davoust CE; Hoffman BM Ligand spin densities in blue copper proteins by Q-band ^1H and ^{14}N ENDOR spectroscopy. *J. Am. Chem. Soc* 1991, 113, 1533–1538.
- (31). Bruggemann W; Niklas JR Stochastic ENDOR. *J. Magn. Reson., Ser. A* 1994, 108, 25–29.
- (32). Doan PE Combining steady-state and dynamic methods for determining absolute signs of hyperfine interactions: Pulsed ENDOR Saturation and Recovery (PESTRE). *J. Magn. Reson* 2011, 208, 76–86. [PubMed: 21075026]
- (33). Yuan H; Collins MLP; Antholine WE Low-frequency EPR of the copper in particulate methane monooxygenase from *Methylobacterium albus* BG8. *J. Am. Chem. Soc* 1997, 119, 5073–5074.
- (34). Lemos SS; Collins MLP; Eaton SS; Eaton GR; Antholine WE Comparison of EPR-visible Cu^{2+} sites in pMMO from *Methylococcus capsulatus* (Bath) and *Methylobacterium album* BG8. *Biophys. J* 2000, 79, 1085–1094. [PubMed: 10920038]
- (35). Peng W; Qu X; Shaik S; Wang B Deciphering the oxygen activation mechanism at the Cu_C site of particulate methane monooxygenase. *Nat. Catal* 2021, 4, 266–273.
- (36). Peisach J; Blumberg WE Structural implications derived from the analysis of electron paramagnetic resonance spectra of natural and artificial copper proteins. *Arch. Biochem. Biophys* 1974, 165, 691–708. [PubMed: 4374138]
- (37). Pogni R; Baratto MC; Diaz A; Basosi R EPR characterization of mono(thiosemicarbazones) copper(II) complexes. *Note II. J. Inorg. Biochem* 2000, 79, 333–337. [PubMed: 10830885]
- (38). Chang W-H; Lin H-H; Tsai I-K; Huang S-H; Chung S-C; Tu I-P; Yu SS-F; Chan SI Copper centers in the cryo-EM Structure of particulate methane monooxygenase reveal the catalytic machinery of methane oxidation. *J. Am. Chem. Soc* 2021, 143, 9922–9932. [PubMed: 34170126]
- (39). Atherton NM; Horsewill AJ Proton ENDOR of $\text{Cu}(\text{H}_2\text{O})_6^{2+}$ in $\text{Mg}(\text{NH}_4)_2(\text{SO}_4) \cdot 4.6\text{H}_2\text{O}$. *Mol. Phys* 1979, 37, 1349–1361.
- (40). Burns CS; Aronoff-Spencer E; Dunham CM; Lario P; Avdievich NI; Antholine WE; Olmstead MM; Vrielink A; Gerfen GJ; Peisach J; Scott WG; Millhauser GL Molecular features of the copper binding sites in the octarepeat domain of the prion protein. *Biochemistry* 2002, 41, 3991–4001. [PubMed: 11900542]
- (41). Kim D; Kim NH; Kim SH 34 GHz pulsed ENDOR characterization of the copper coordination of an amyloid β peptide relevant to Alzheimer's disease. *Angew. Chem., Int. Ed* 2013, 52, 1139–1142.
- (42). Fujimoto M; McDowell CA; Takui T Ligand ENDOR spectra of Cu(II) impurity complexes in α -glycine crystals. *J. Chem. Phys* 1979, 70, 3694–3701.
- (43). Rist GH; Hyde JS Ligand ENDOR of metal complexes in powders. *J. Chem. Phys* 1970, 52, 4633–4643.
- (44). Manikandan P; Epel B; Goldfarb D Structure of copper(II)-histidine based complexes in frozen aqueous solutions as determined from high-field pulsed electron nuclear double resonance. *Inorg. Chem* 2001, 40, 781–787. [PubMed: 11225123]
- (45). Vancamp HL; Sands RH; Fee JA Electron-nuclear double-resonance on copper(II) tetraimidazole. *J. Chem. Phys* 1981, 75, 2098–2107.
- (46). Liew EF; Tong DC; Coleman NV; Holmes AJ Mutagenesis of the hydrocarbon monooxygenase indicates a metal centre in subunit-C, and not subunit-B, is essential for copper-containing membrane monooxygenase activity. *Microbiology* 2014, 160, 1267–1277. [PubMed: 24682027]
- (47). Frandsen KE; Simmons TJ; Dupree P; Poulsen JC; Hemsworth GR; Ciano L; Johnston EM; Tovborg M; Johansen KS; von Freiesleben P; Marmuse L; Fort S; Cottaz S; Driguez H; Henrissat B; Lenfant N; Tuna F; Baldansuren A; Davies GJ; Lo Leggio L; Walton PH The molecular basis of polysaccharide cleavage by lytic polysaccharide monooxygenases. *Nat. Chem. Biol* 2016, 12, 298–303. [PubMed: 26928935]
- (48). Elwell CE; Gagnon NL; Neisen BD; Dhar D; Spaeth AD; Yee GM; Tolman WB Copper-oxygen complexes revisited: structures, spectroscopy, and reactivity. *Chem. Rev* 2017, 117, 2059–2107. [PubMed: 28103018]

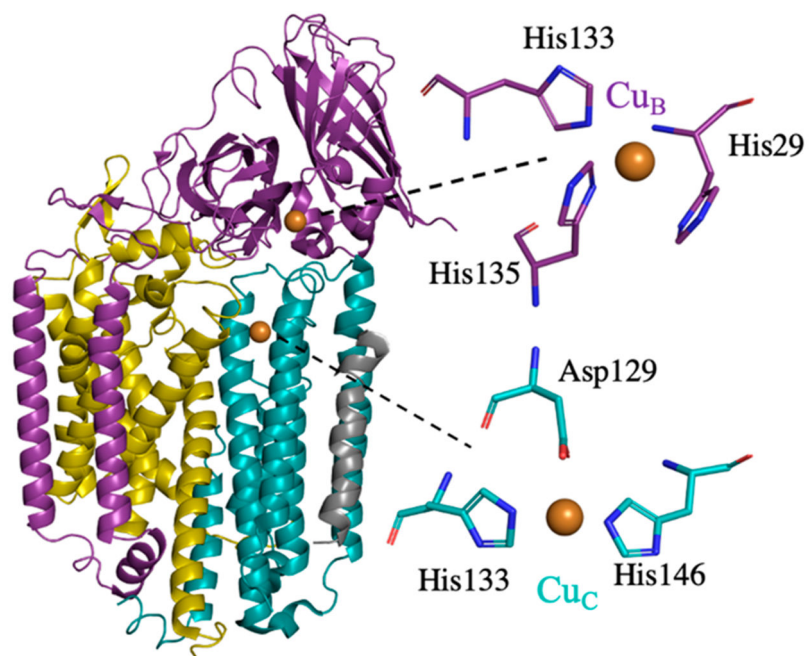


Figure 1. A single protomer from the crystal structure of *Mc. sp. str. Rockwell* pMMO (PDB accession code 4PHZ). PmoA is light gold, PmoB is purple, PmoC is teal, and an unidentified helix is gray. The two copper ions are shown as spheres and to the right are expanded to show the modeled coordinating residues.

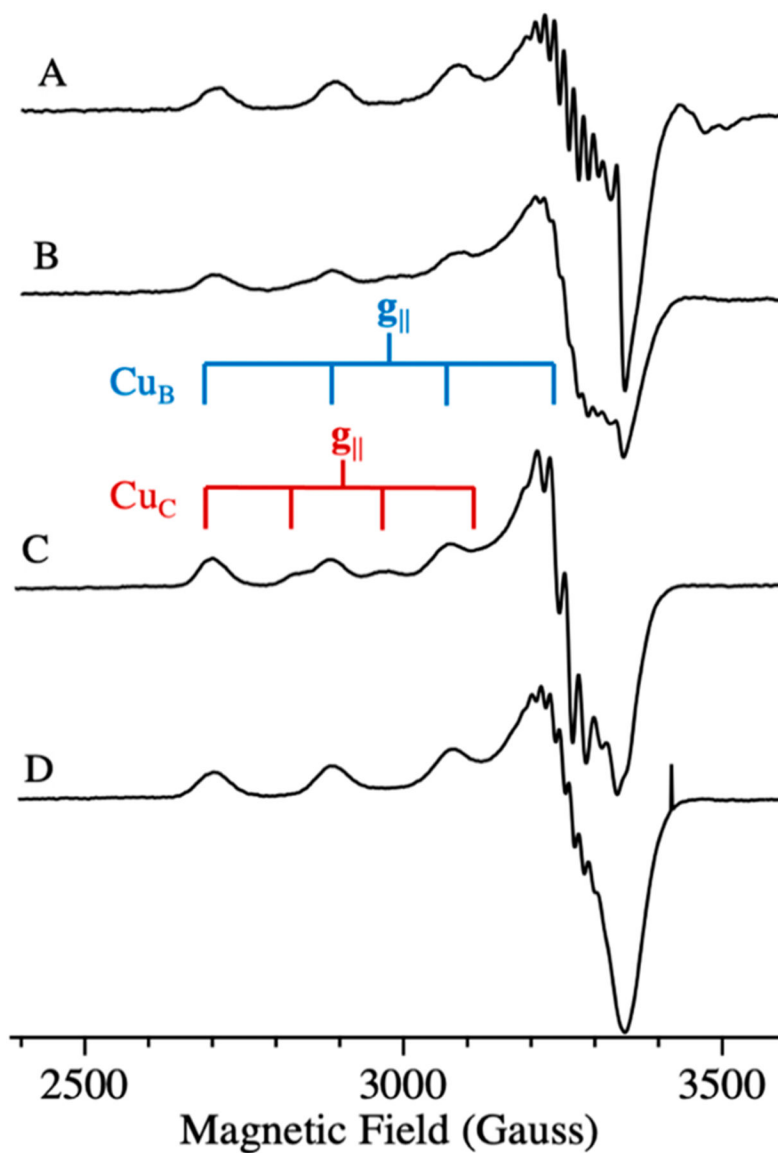


Figure 2. CW X-band EPR spectra of *Mc. sp. str.* Rockwell pMMO. (A) In vivo pMMO. (B) Membrane-bound pMMO. (C) Purified pMMO. The brackets indicate the ^{63}Cu $A_{||}$ hyperfine splitting of the two signals present in the spectra. (D) Purified/reduced pMMO. Conditions: 9.36 GHz microwave frequency, 200 μW MW power, temperature 20 K, 320 ms time constant, 12.5 G modulation, 5 scans each, and 10 G/s scan rate.

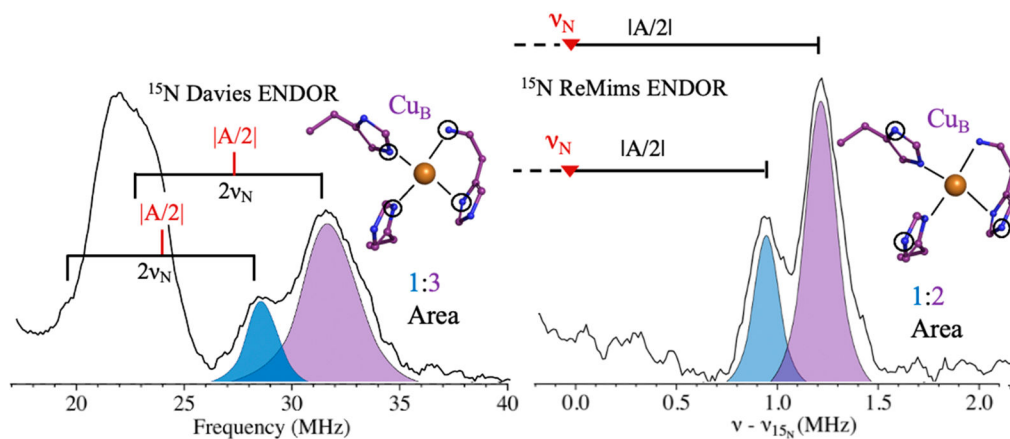


Figure 3.

The 2 K Q-band ^{15}N pulsed ENDOR on the *Mc. sp. str. Rockwell* in vivo pMMO Cu_B site. (Left) Pulsed Davies ENDOR spectra at $g = 2.25$ of directly coordinated ^{15}N . The brackets represent twice the ^{15}N Larmor frequency and are centered at the value of $|A/2|$ (red). (Right) Doan/ReMims spectra at $g = 2.24$ for distally coupled ^{15}N (“backside nitrogen”), ^{15}N Larmor subtracted for centering. The solid right bracket represents $|A/2|$, where the red \blacktriangledown represents the ^{15}N Larmor frequency. To show the analysis better, the ν -peaks are omitted, but see below. Davies ENDOR conditions: 34.684 GHz, 100 ms repetition time, $\pi = 80$ ns, $\tau = 600$ ns, TRF = 35 μs , RF tail = 5 μs , ~ 100 scans. ReMims conditions: 34.712 GHz, 20 ms repetition time, $\pi = 60$ ns, $\tau_1 = 200$ ns, $\tau_2 = 400$ ns, TRF = 60 μs , and RF tail = 10 μs .

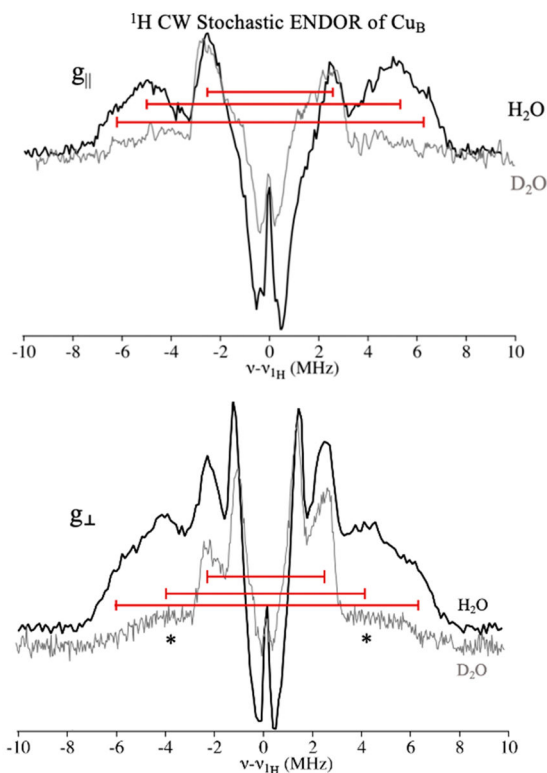


Figure 4.

Mc. sp. str. Rockwell in vivo pMMO Cu_B site Q-band 2 K stochastic ¹H ENDOR at fields corresponding to $g = 2.31$ (top) and $g = 2.02$ (bottom). The gray trace is D₂O exchanged samples at the same fields. Asterisks denote ⁶³Cu ENDOR response that underlies the ¹H pattern. The stochastic sequence enhances resolution, and resolved couplings are shown by the brackets, the length of which represents the value of A (see the text). Conditions: 34.78 GHz, 4 G modulation, 1 μ W MW power, 2 s rf on, 2 s rf off, 0.5 s wait time, ~2000 scans each.

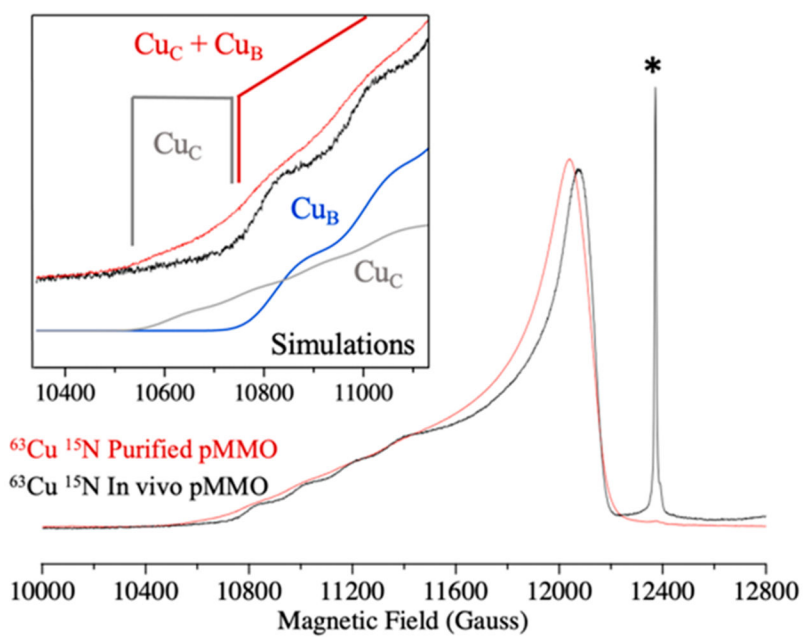


Figure 5. The 2 K Q-band absorption EPR with the spectra of in vivo (black) and purified (red) *Mc. sp. str. Rockwell* pMMO overlaid. At this frequency, the $+^{3/2}$ ^{63}Cu hyperfine of the Cu_C site is separated from the Cu_B site, as also shown by individual simulations of the two sites (inset). The asterisk marks a radical that is present in whole-cell samples. Conditions: ~ 34.8 MHz, 1 G modulation, 1 μW MW power, 128 ms time constant, 20 G/s sweep rate.

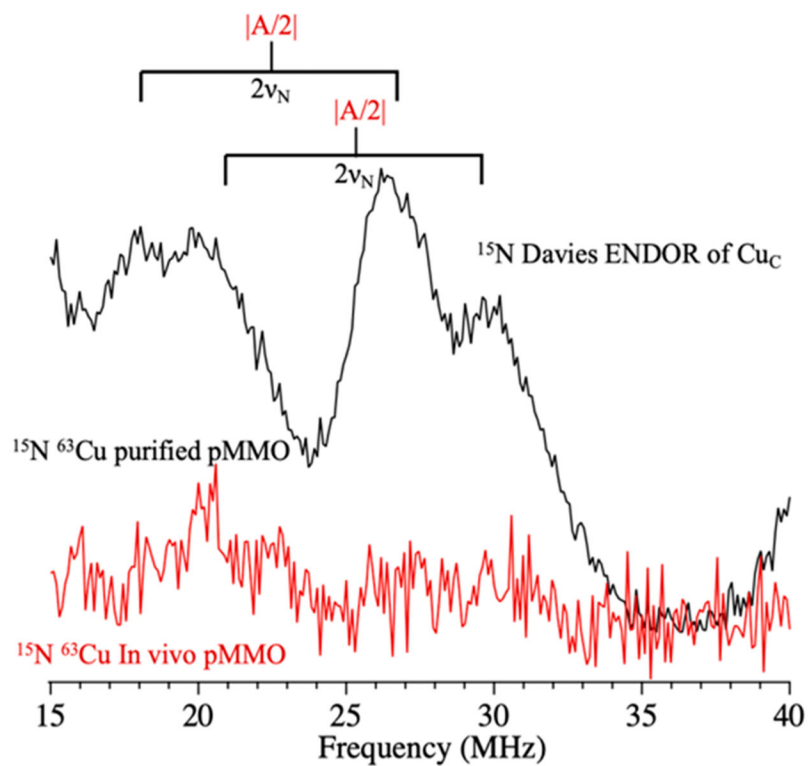


Figure 6. Q-band Davies pulsed ¹⁵N ENDOR at a field corresponding to $g = 2.32$ for purified (black) and in vivo (red) *Mc. sp. str. Rockwell* pMMO. The brackets represent twice the ¹⁵N Larmor frequency and are centered at the value of $|A/2|$. Conditions: 2 K, 34.684/34.774 GHz, 100 ms repetition time, $\pi = 80$ ns, $\tau = 600$ ns, TRF = 35 μ s, RF tail = 5 μ s, ~100 scans.

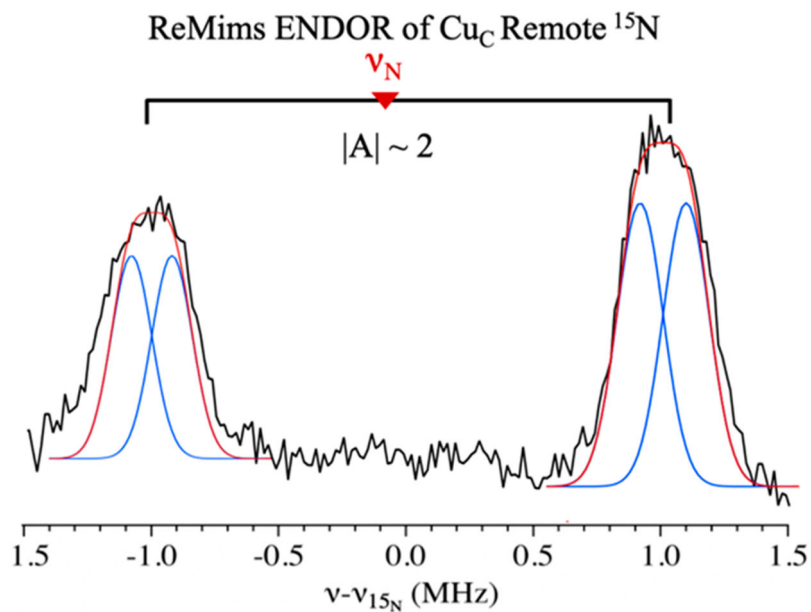


Figure 7. Q-Band Doan/ReMims ¹⁵N pulsed ENDOR at 10 700 G ($g = 2.32$) for purified ⁶³Cu ¹⁵N *Mc. sp. str. Rockwell pMMO* (black). The bracket represents $|A|$ for the remote ¹⁵N couplings and the spectrum is centered on the ¹⁵N Larmor frequency. The breadth of the individual peaks is much larger than the widths of the individual responses for Cu_B, which suggests that multiple ¹⁵N couplings are overlapped. The spectrum was fit to the overlap of two ¹⁵N doublets for which individual peaks were taken to have the same widths of the individual remote ¹⁵N of Cu_B (Figure 3, right).

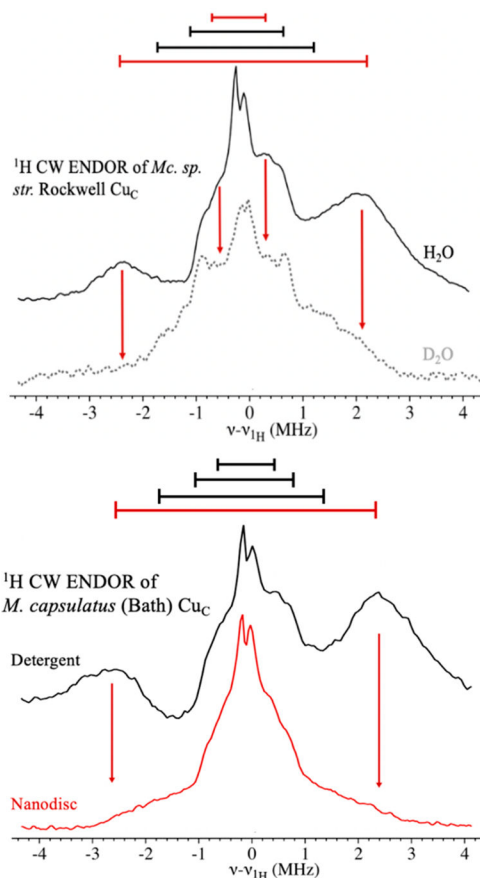


Figure 8. (Upper) Q-band CW ^1H ENDOR spectra of the *Mc. sp. str. Rockwell* pMMO Cu_C site (10 650 G). Black trace, purified pMMO in H_2O ; dotted gray trace, purified pMMO in D_2O . Red arrows indicate the loss of the ~ 5 and ~ 1 MHz couplings upon D_2O exchange. Conditions: 34.8 GHz microwave frequency, 4 G modulation, 32 ms TCs, $1 \mu\text{W}$ MW power, forward sweep, ~ 75 scans, 0.25 MHz/s. (Lower) Q-Band CW ^1H ENDOR of the Cu_C site of purified *M. capsulatus* (Bath) pMMO in detergent (black) and in a nanodisc (red). Red arrows indicate the absence in the nanodisc of the $A \sim +5$ MHz coupling assigned as a distal water, seen also in measurements on detergent-purified *Mc. sp. str. Rockwell* pMMO. The conditions are identical to those in Figure 7, except the nanodisc sample, with a lower enzyme concentration, required ~ 400 scans.

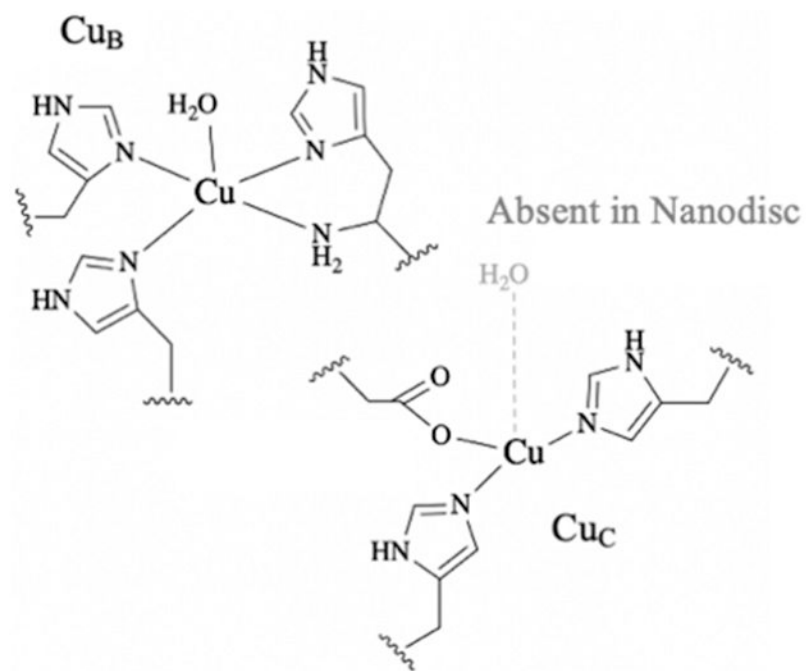


Figure 9.
Current models for the two copper sites of pMMO.